*J Mater Sci: Mater Electron* (2021) 32:28587–28604

# Homovalent Ho/Bi substitution effect on characteristic properties of Bi-2212 superconducting ceramics

Umit Erdem[1,*]

[1] *Scientific and Tech. Research Center, Kirikkale University, 71450 Kirikkale, Turkey*

**Received:** 9 August 2021
**Accepted:** 12 October 2021
**Published online:** 23 October 2021



## ABSTRACT

In the current work, the effect of trivalent Ho/Bi partial replacement on the fundamental characteristic features such as the general crystallinity quality quantities, dc electrical resistivity, superconducting, degree of granularity, strength quality of intra- and inter-grain boundary couplings in the oxygen-deficit multi-layered perovskite-based $Bi_{2.1}Sr_{2.0}Ca_{1.1}Cu_{2.0}O_y$ (Bi-2212) superconducting ceramics is examined by powder X-ray diffraction (XRD), temperature-dependent electrical resistivity ($\rho$-T), and Archimedes water displacement methods. The polycrystalline $Bi_{2.1-x}Ho_xSr_{2.0}Ca_{1.1}Cu_{2.0}O_y$ compounds are produced by the conventional ceramic method within the molecular ratio intervals $0.00 \leq x \leq 0.30$. All the experimental findings show that the trivalent holmium ($Ho^{3+}$) impurities are successfully substituted by the bismuth ($Bi^{3+}$) particles in the Bi-2212 crystal system. Besides, the optimum holmium concentration for the bulk Bi-2212 superconducting ceramics is recorded to be $x = 0.01$. XRD results indicate that the Bi-2212 material prepared by the optimum Ho/Bi substitution possesses the maximum average crystallite size (60 nm), Bi-2223 superconducting phase volume fraction (33.48%), *c*-axis length (32.55 Å), and Lotgering index (0.48) parameters. In this respect, the best sample with particle distributions well linked each other has the maximum bulk density value of 6.04 $g/cm^3$ and minimum degree of granularity of 4.13%. It is obvious that the optimum (excess) Ho/Bi partial substitution supports the enhancement in the density (granular structure nature) of Bi-2212 compound. Moreover, dc electrical resistivity measurement results show that the optimum homovalent Ho/Bi partial substitution in the Bi-2212 superconducting matrix leads to increase the homogeneities in the oxidation state of superconducting grains and especially densities of active and effective electronic states (DOS) at Fermi energy level. To sum up, this study indicates that the optimum trivalent Ho/Bi partial substitution increases the usage of Bi-2212 superconducting materials in much more application fields.

Address correspondence to E-mail: umiterdem@kku.edu.tr

https://doi.org/10.1007/s10854-021-07236-z

## 1 Introduction

On the discovery of superconductivity with the metal solid of mercury element at the temperature of 4.2 K in 1911 [1], the concept and quest of superconducting materials have attracted a great deal of interest of research community worldwide. With the discovery of new parents including new elements, pure and semi-metals, alloys, nickelates, pyrochlore oxides, compounds (carbon-, organic-, heavy fermion-, inorganic-, chalcogen-, iron-, semi-metal, chevrel phase- and silicon-containing), A-15 compounds, carbonaceous sulfur hydride, lanthanum decahydride, rare-earth borocarbide, rutheno-cuprates, magnesium diboride, and cuprate types (Tl-, Bi-, and Hg-based high-Tc superconducting compounds) over time the interest in the field has continuously increased [2, 3]. The main reason for the increased interest stems from the intrinsic superior characteristics such as high current density and magnetic field carrying capability, energy consumption and losses without any (or less) power consumption, and energy dissipations based on the Joule effect in the application fields [4]. Today, the superconducting materials are separated into two main parts: (i) soft type-I and (ii) hard type-II ceramic compounds [5–7]. The parents of soft type-I are the conventional superconductors and generally composed of the pure elements and alloys. On the other hand, the second parents of ceramic compounds consist of the copper oxide (distorted, oxygen deficient) multi-layered perovskite materials and work above the temperature of 77 K (boiling point of liquid nitrogen). The former materials have extensively been used in the practical applications before the discovery of high-temperature ones. However, today the latter type superconductors are preferred to use in the advanced engineering, power transmission cable, medical diagnosis, heavy-industrial technology, future cryo/refrigeration and hydrogen society, and large-scale applications [8–11] due to their own extremely greater critical transition temperature, magnetic field, and engineering current carrying ability [12, 13]. Similarly, higher thermodynamic stability, cheap contents, easy preparation process, non-toxic chemicals, accessible of nitrogen for the cooling system, resistant towards to the water/humid atmosphere, stability towards to the compositional content and oxygen, small power consumption, and dissipations are important properties [12–16].

The type-II ceramic compounds are also called as cuprates due to the presence of Cu-$O_2$ superconducting layers separated by spacer layers and the superconducting features are defined by mobile carriers (electrons or holes) moving within weakly coupled Cu-$O_2$ layers. According to the phase diagram, the cuprate superconductors are divided into two main types including the electron and hole-doped cuprates. The standard superconductors such as Y- and Bi-based superconductors (the most studied materials in the literature) are known to be hole-doped cuprate compounds [17]. With the dopant atoms, the number of mobile carriers can be refined considerable. This means that some problematic characteristics such as lower operating temperature intervals, spatial characteristic of mobile carriers, layered anisotropic structure in normal conducting and superconducting properties, sensitivity to applied magnetic fields and current, inter-granular boundary, stabilization of characteristic phases (presence of three or more phases together in the system), randomly oriented microcrystals, structural problems, multiple-phase compositions, brittleness behavior, mechanical stabilization, weak coupling problems between the superconducting grains, extreme-short coherence length, enormously large penetration depth, and low charge carrier densities can be improved for increasing the usage of superconducting ceramic cuprates in much more application fields [18, 19]. The problems mentioned can extensively be overcome by cation/anion substitutions, chemical addition, and doping mechanism in the crystal structure due to effective contribution of dopant ions on the main characteristic quantities including the electrical conductivity, superconducting, bulk density, flux pinning ability, crystallinity quality, structural morphology, and strength quality of connection between the grains in the superconducting matrix [20–22].

The Bi-containing family (one of the most preferred members in the cuprate parents in the usage of advanced engineering, heavy-industrial technology, and large-scale application fields) crystallizes in the tetragonal crystal structure and possesses 3 main superconducting phases homologous series as $Bi_2Sr_2Ca_{n-1}Cu_nO_{4+2n+x}$ ($n$ = 1, 2, and 3). The number of $n$ points out the effective and active Cu–$O_2$ consecutively stacked layers and Ca layers in the unit cell [23, 24]. On this basis, three phases abbreviated with respect to the number of $n$ are Bi-2201, Bi-2212, and

Bi-2223. The former phase obtains the lowest critical transition temperature of 20 K whereas the latter one exhibits the maximum critical transition temperature of 110 K [25, 26]. Similarly, the *c*-axis length presents the similar trend (constant increase with the number of *n*) and the maximum length of 37.1 Å is observed for the characteristic Bi-2223 superconducting phase. In this context, the increment in the active $Cu–O_2$ - consecutively stacked layers and Ca layers in the unit cell leads to promote dramatically the enhancement of superconducting transition temperature and *c*-axis length parameters. However, it is to be mentioned here that the Bi-2212 superconducting phase with the critical transition temperature of 85 K is relatively simpler formed as compared to the single phase of Bi-2223. Besides, the superconducting compound with larger fraction of Bi-2223 phase can be prepared after a long sintering time of more than a week at the temperature of 870 °C [27]. On this basis, the interest of researchers has greatly been attracted by the characteristic Bi-2212 superconducting phase.

Holmium ($Ho^{3+}$), as a chemical element, is a rare-earth metal of the lanthanide series of the periodic table [28]. Holmium has the highest magnetic moment (10.6 μB) of any naturally occurring element and has other unusual magnetic properties [29]. Holmium has the highest magnetic strength of any element and is, therefore, used to create the strongest artificially created magnetic fields when placed inside high-power magnets as a magnetic pole piece (also called a magnetic flux concentrator) [30]. The addition of rare earth in high-temperature superconductors such as YBCO and BSCCO leads to significant changes in microstructural, electrical, and mechanical properties [31]. Rare earth can exhibit ferromagnetic, antiferromagnetic, and paramagnetic properties at different temperatures as a result of the electron joining the 4f orbital [31]. For example, $Ho^{3+}$ exhibits ferromagnetic properties below 20 K, antiferromagnetic between 20 and 133 K, and paramagnetic above 133 K [32]. However, $Ho^{3+}$ ions have been reported to be the most magnetically optically active ions [33]. It is also reported that amphoteric rare-earth ions with Ho medium ionic radius provide good electrical properties and high reliability to bismuth ($Bi^{3+}$) ceramics [34]. It is known that the Ho-doped sample shows a low condensation rate [35]. In addition, in a study conducted with the addition of Ho, researchers obtained the result that crystallites with monoclinic structure completely disappeared and a pure tetragonal structure was formed [36]. It has been reported that $Ho^{3+}$ is advantageous in obtaining less cracks and higher densities in microstructures, since it has an effect on limiting crystal growth. Therefore, $Ho^{3+}$ among the rare-earth elements is the most promising materials for potential technological and industrial applications.

In the current work, we examine the role of different partial homovalent substitution levels ($0.00 \leq x \leq 0.30$) of $Ho^{3+}$ particles for the $Bi^{3+}$ impurities in the Bi-sites of $Bi_{2.1}Sr_{2.0}Ca_{1.1}Cu_{2.0}O_y$ (Bi-2212) superconducting ceramic compound with the highest stability and thermodynamic properties on the fundamental characteristic features; namely, the electrical resistivity, superconducting, bulk density, crystal structure quality, and strength quality of connectivity between the grains with the aid of powder X-ray diffraction, temperature-dependent electrical resistivity, and Archimedes water displacement methods. Similarly, the experimental measurement findings are extensively discussed by the theoretical approaches. All the findings indicate that the fundamental characteristic features are found to refine seriously with the optimum trivalent Ho/Bi substitution level of $x = 0.01$.

## 2 Experimental procedures for preparation of Bi-2212 ceramic compounds

In the current study, the conventional solid-state reaction method is used to prepare the $Bi_{2.1-x}Ho_xSr_{2.0}Ca_{1.1}Cu_{2.0}O_y$ materials within the molecular ratio intervals $0.00 \leq x \leq 0.30$ to minimize the serious crystallinity problems including the experimental syntactic intergrowth, microscopic cracks, randomly or misoriented microcrystals, porosity, impurity residues, microvoid/grain coalescences, lattice strains, internal, and structural omnipresent defects (Schottky, Frenkel, and off-center ions as the point defects; edge and screw dislocations as the line defects; grain boundaries and stacking faults as the planar defects; cracks, voids, and pores as the bulk defects) in the crystal structure. All the preliminary stages (processes of weighing, mixing, milling, etc.) are exerted in the atmospheric air at the room temperature. For the production of Ho/Bi partial-replaced ceramic compounds, the high-purity (≥ 99.99%) precursor chemical powders of $Bi_2O_3$,

$Ho_2O_3$, $SrCO_3$, CuO, and $CaCO_3$ purchased from an exclusive distributor of Alfa Aesar products are used. The chemical in the powders is separately weighed as the raw materials (~ 2.8 mg in total) in a mole-to-mole ratio of $2.1-x:x:2.0:1.1:2.0$ ($Bi_{2.1-x}Ho_xSr_{2.0}Ca_{1.1}Cu_{2.0}O_y$) within the various molecular weight ratios between 0 and 1% using the electronic balance and is gathered together in 6 different crossing bowls. Raw chemical of powders is exposed to the mixing process in the grinding machine during the period of 9 h to obtain homogenous mixture of powders and decrease the particle sizes of chemicals to the desired size. The mixture of powders is manually grounded by a grinder for 30 min in an agate mortar without any solvent or solution so that the particles bring closer to each other and, thus, the inter-particle bonds more and more strengthen. The last form of powders is calcined in a standard ashing furnace at 800 °C for 36 h under the atmospheric air condition with a heating rate of 5 °C/min to release the impurity residuals based on the carbon or carbon-containing contents from the nominal compositions of $Bi_{2.1-x}Ho_xSr_{2.0}Ca_{1.1}Cu_{2.0}O_y$ ceramic compounds. The heating processes are performed in the porcelain crucibles due to their non-reactive and heat resistant characteristic feature. Besides, the temperature of furnace is reduced with a cooling rate of 5 °C/min to the room temperature. The color of resultant powders removed from the furnace turns into blackish. The powders calcined are again reground in the agate mortar to reach both the maximum homogeneity and optimum size of chemicals [37]. The final form of chemicals is molded with the aid of 300 MPa load into a rectangular bar with the volume size of $1.5 \times 0.5 \times 0.2$ $cm^3$ to minimize the number of voids and superconducting grain boundary coupling problems. The solid rectangular bars with nominal composition of $Bi_{2.1-x}Ho_xSr_{2.0}Ca_{1.1}Cu_{2.0}O_y$ are subjected to the main heating process (providing the Bi-2212 characteristic superconducting phase) at 850 °C for 24 h using the same heating and cooling rates. In the current work, thereafter, the Bi-site Ho replaced Bi-2212 superconducting ceramics prepared with the various Ho content levels such as $x$ = 0.00, 0.01, 0.03, 0.05, 0.07, and 0.10 will be presented as pure, Ho/Bi-1, Ho/Bi-2, Ho/Bi-3, Ho/Bi-4, and Ho/Bi-5, respectively.

## 3 Characterization for $Bi_{2.1-x}Ho_xSr_{2.0}Ca_{1.1}Cu_{2.0}O_y$ ceramic compounds

In the present study, the characterization of prepared $Bi_{2.1-x}Ho_xSr_{2.0}Ca_{1.1}Cu_{2.0}O_y$ ceramic compounds is extensively carried out by the conventional identification methods, viz., the bulk density grounded on Archimedes water displacement method for the determination of structural defects in the short-range-ordered antiferromagnetic active $Cu–O_2$ consecutively stacked layers and especially change in the voids, superconducting grain boundary coupling problems, and interaction between the superconducting grains; powder XRD measurements for phase volume fractions, crystallinity quality, average crystallite sizes, lattice strains, Lotgering indices, lattice cell parameters, grain alignment (texturing) distributions, and orientations; temperature-dependent dc electrical resistivity measurements for normal state resistivities, residual resistivities, residual resistivity ratios, some important resistivity parameters such as $\rho_{norm}$, $\rho_{90K}$, and $\Delta\rho$.

Bulk density tests are experimentally performed by means of simple Archimedes water displacement method and the corresponding granularity degrees (residual porosities) are evaluated from the measurement findings. Moreover, change in the electrical resistivity against environment temperatures for the materials studied is deduced form the conventional four-probe method in a He closed cycle cryogenic system under vacuum condition. Experimental signals are recorded from the temperature of 35 K until 105 K in the presence of 5 mA dc current driven along the surface and the accuracy is recorded to about ± 0.01 K by a programmable nano-voltmeter and current source. At the same time, the general crystal structure quantities are searched by a SHIMADZU 6000 XRD diffractometer emitting wavelength of 1.544 Å (produced by 40 kV/40 mA) for the $K_\alpha$ line of Cu. The experimental signals are gathered in the $2\theta$ angles of 3°–60° with 0.1° step increment. JCPDS index cards with JCPD-ICDD numbers of 41-0317 and 41-0374 are used for the indexation of well-defined diffraction peaks in the XRD diffractograms.

## 4 Results and discussion

### 4.1 XRD experimental measurement results

In the present work, the fundamental influence of trivalent Ho/Bi partial substitution in the bulk Bi-2212 superconducting system on the general crystallinity quantities such as the crystallinity quality, crystallization system, phase volume fractions, average crystallite sizes, lattice strains, Lotgering indices, lattice cell parameters, grain alignment (texturing) distributions, and orientations is investigated by using the powder XRD measurements. The diffraction patterns in the XRD diffractograms are recorded in a range of 3°–60° and depicted in Fig. 1. According to the XRD plots, the $Bi_{2.1-x}Ho_xSr_{2.0}Ca_{1.1}Cu_{2.0}O_y$ ceramic compounds with the polycrystalline crystal structure show the crystalline solid feature (long-range atomic arrangement in a highly ordered microscopic structure extended with 3D periodicity network in all directions). Further, it is obvious that the increment in the holmium impurity in the polycrystalline perovskite-based Bi-2212 superconducting system leads not only to shift the diffraction peaks with the diffraction intensities to the low/high angles in the XRD diffractograms but also to appear or disappear new diffraction peaks. The variation of XRD patterns with the Ho/Bi partial substitution level claims that the trivalent holmium impurities are successfully substituted in the Bi-site Bi-2212 superconducting matrix. Moreover, the characteristic superconducting peaks diffracted from the beams are named with respect to Miller indices of *VL* (*hkl*), *L* (*hkl*), and *H* (*hkl*). Here, the first characteristic peaks stemming from very low phase are attributed to Bi-2201 superconducting system. *L* (*hkl*) and *H* (*hkl*) are low superconducting phase (Bi-2212 superconducting material) and high superconducting phase (Bi-2223 system), respectively. Besides, the experimental findings show that the oxygen-deficit multi-layered perovskite-based $Bi_{2.1-x}Ho_xSr_{2.0}Ca_{1.1}Cu_{2.0}O_y$ ceramic compounds crystallize in the tetragonal space group $P_{4/mmm}$ (negligible orthorhombic distortion). The related diffraction peaks are indexed with regard to the JCPD-ICDD numbers of 41-0317 and 41-0374 in the JCPDS index cards. It is apparent from the XRD diffractograms that the $Bi_{2.1-x}Ho_xSr_{2.0}Ca_{1.1}Cu_{2.0}O_y$ materials every exhibit low Bi-2212 and high Bi-2223 superconducting phases together despite the different volume fraction ratios within the crystal system (discussed below). The co-occurrence of Bi-2212 and high Bi-2223 in the perovskite-based Bi-2212 superconducting crystal system is natural. It is to be mentioned here that the formation velocity of high Bi-2223 superconducting phase is found to increase slightly for the Ho/Bi substitution level of $x = 0.01$ after which the high phase tends to reduce systematically with the augmentation in the

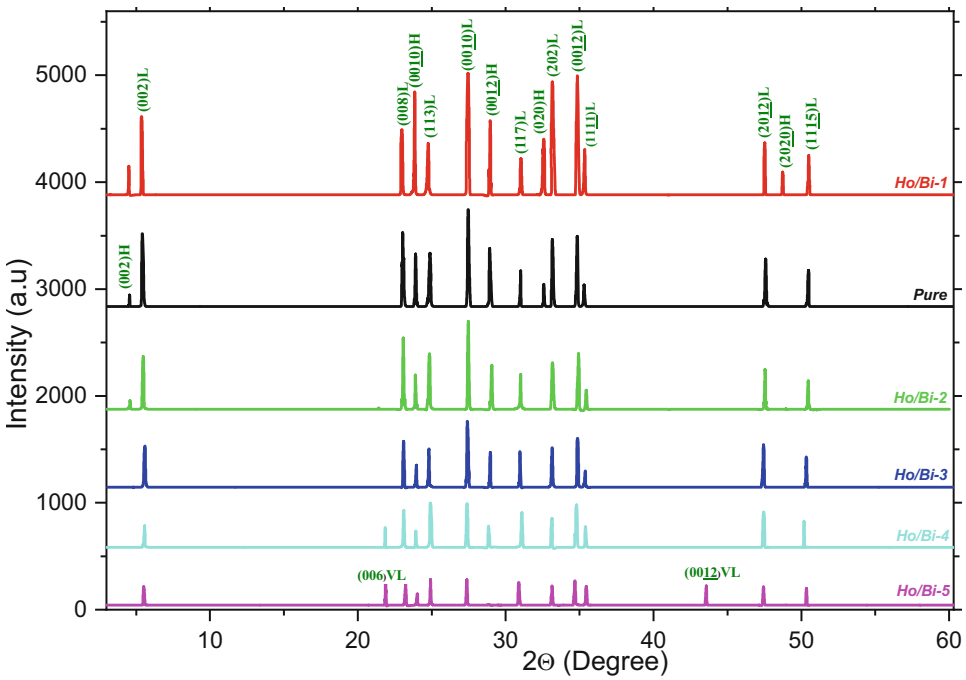


**Fig. 1** Experimental Diffraction patterns for pure and Ho/Bi partial-replaced Bi-2212 superconductors. Notations of "*H*," "*L*," and "VL" display the characteristic superconducting phases of Bi-2223, Bi-2212, and Bi-2201, respectively

homovalent Ho/Bi partial replacement level in the Bi-2212 crystal system. On the other hand, the formation velocity of low Bi-2212 superconducting phase in the crystal structure accelerates up the certain Ho/Bi substitution level of $x = 0.05$ due to the degradation in the high Bi-2223 superconducting phase. However, after the critical replacement value, new family member of Bi-2201 superconducting phase formation begins in the system. In case of maximum cationic substitution level of trivalent Ho/Bi, Bi-2201 phase becomes more and more predominantly. Thus, the existence of both Bi-2223 and especially Bi-2212 superconducting phases diminishes harshly. The visual findings can enable us to interpret the fact that the presence of excess holmium in the bulk Bi-2212 superconducting crystal lattice causes the serious crystallinity problems. Regardless, among the phases, the Bi-2212 superconducting phase is evident and strongest; hence, no impurity phase can prevent the formation of thermodynamically activated super-electrons (effective and strong electron–phonon coupling probabilities) in the homogeneous superconducting cluster percentages in the paths, being already discussed by the following parts based on the dc electrical resistivity results. Moreover, it is to be stressed here that in all the XRD diffractograms, there is no peak related different phases including Ho impurity or Ho-based other cations. This is attributed to the fact that the Ho impurity is completely solved in the polycrystallized Bi-2212 superconducting crystal structure [38, 39].

Additionally, the diffraction peaks in the XRD diffractograms guarantee that the family participants of Bi-2223 and Bi-2201 superconducting phases present the low reflection intensities while those of Bi-2212 superconducting phase are associated with the strong intensities. On this basis, the diffraction peak intensities for the characteristic Bi-2212 and Bi-2223 phase are observed to be rather stronger depending on the enhancement of crystallinity quality as the aliovalent Ho/Bi partial substitution level is $x = 0.01$. On the other hand, from the critical substitution level of $x = 0.01$ onwards, the peak intensities of Bi-2212 and especially Bi-2223 superconducting phase are recorded to degrade seriously and reach the minima points for maximum substitution level. However, the peak intensities of Bi-2201 superconducting phase begin to appear immediately at the replacement level of $x = 0.07$ and above. In fact, the intensities tend to increase dramatically with the Ho/Bi partial substitution and reach to the maximum points for the highest dopant level of $x = 0.10$. On this basis, we calculate the relative phase volume fractions within percentages for the Bi-2223, Bi-2212, and Bi-2201 superconducting phases using the relations depicted as follows:

$$f_{(2223)} = \frac{\sum I_{2223(hkl)}}{\sum I_{2223(hkl)} + \sum I_{2212(hkl)} + \sum I_{2201(hkl)}} \times 100\%, \quad (1)$$

$$f_{(2212)} = \frac{\sum I_{2212(hkl)}}{\sum I_{2223(hkl)} + \sum I_{2212(hkl)} + \sum I_{2201(hkl)}} \times 100\%, \quad (2)$$

$$f_{(2201)} = \frac{\sum I_{2201(hkl)}}{\sum I_{2223(hkl)} + \sum I_{2212(hkl)} + \sum I_{2201(hkl)}} \times 100\%. \quad (3)$$

in the equations, $I$ shows the diffraction peak intensity of Bi-2223, Bi-2212, and Bi-2201 superconducting phases. One can see all the numerical computations in Table 1. It is visible from the table that the pure, Ho/Bi-1, Ho/Bi-2, and Ho/Bi-3 samples obtain Bi-2212 and Bi-2223 superconducting phases whereas the last two compounds possess the extra Bi-2201 superconducting phases in their crystal system. Numerically, the pure sample presents the volume fraction values of 79.70% and 20.30% for the Bi-2212 and Bi-2223 superconducting phases, respectively. Besides, the bulk Ho/Bi-1 sample exhibits the Bi-2223 phase value of 33.48% (maximum value among the materials studied) as against 66.52% for the Bi-2212 superconducting phase in the crystal structure. In this respect, the optimum Ho/Bi substitution not only favors the Bi-2223 superconducting phase but also enables stabilize the Bi-2212 superconducting phase in the oxygen-deficit multi-layered perovskite-based $Bi_{2.1-x}Ho_xSr_{2.0}Ca_{1.1}Cu_{2.0}O_y$ ceramic compounds. In case of optimum holmium concentration level of $x = 0.01$ in the crystal structure, the Ho particles provide an available medium to convert the Bi-2212 superconducting phase to the Bi-2223 phase. On the other hand, it can be discussed that while the presence of excess Ho particles in the Bi-2212 crystal system damages considerably the Bi-2223 superconducting phase, the characteristic Bi-2201 phase begins to appear immediately and in fact becomes to predominate for the maximum substitution level. In this context, the Bi/Ho-5 sample shows the Bi-2223, Bi-2212, and Bi-2201 phases within the volume ratios of 4.13%, 79.93%, and 15.94%, respectively. The similar trend is also observed in the scientific papers in the literature [40, 41]. To sum up, it is obvious that the

**Table 1** XRD experimental results including phase volume fractions, average crystallite sizes, lattice cell parameters, and Lotgering indices for all the multi-layered perovskite-based $Bi_{2.1-x}Ho_xSr_{2.0}Ca_{1.1}Cu_{2.0}O_y$ superconducting ceramic compounds

| Materials | $a$ (Å) | $c$ (Å) | Volume fraction ( ≈ %) | | | Average grain size (nm) | Lotgering index, F |
|---|---|---|---|---|---|---|---|
| | | | 2212 | 2223 | 2201 | | |
| Pure | 5.36 | 30.66 | 79.70 | 20.30 | 0 | 58 | 0.44 |
| Ho/Bi-1 | 5.32 | 32.55 | 66.52 | 33.48 | 0 | 60 | 0.49 |
| Ho/Bi-2 | 5.38 | 30.48 | 83.56 | 16.44 | 0 | 55 | 0.41 |
| Ho/Bi-3 | 5.40 | 30.39 | 86.90 | 13.10 | 0 | 54 | 0.39 |
| Ho/Bi-4 | 5.43 | 30.24 | 85.22 | 9.68 | 5.10 | 52 | 0.39 |
| Ho/Bi-5 | 5.44 | 30.14 | 79.93 | 4.13 | 15.94 | 51 | 0.37 |

partial cationic substitution amount of $Ho_2O_3$ chemical in the Bi-2212 crystal structure affects remarkably (positive or negative with respect to the dopant level) the formation of superconducting phases in the system. The variation in the formation of superconducting phases stems from the refinement or degradation in the crystallinity problems, being favored by the lattice cell parameters.

In addition to the change of peak intensities of superconducting phases, we also examine the appearance and disappearance of diffraction peaks in the XRD diffractograms. According to the figure, the optimum partial Ho/Bi replacement level of $x = 0.01$ leads to appear new Bi-2223 superconducting phase peak assigned as $H$ (20$\underline{20}$) at $2\theta$ angle of $\sim$ 48.76° in the Bi-2212 crystal structure. However, the peak is observed to disappear for other substitution levels. At the same time, from the Ho/Bi replacement concentration level of $x = 0.30$ onward, the peak indexed as $H$ (*002*) vanishes immediately. It is clear that the excess holmium impurity damages the growth of crystal throughout the (*002*) orientation. The similar situation is observed for the $H$ (*202*) diffraction peak. On this basis, only the pure and Ho/Bi-2 superconducting compounds possess the $H$ (*202*) diffraction peak at $2\theta$ angle of $\sim$ 32.56°–32.57°. Similarly, the diffraction peak indexed as $H$ (*00*$\underline{12}$) disappears for the maximum partial Ho/Bi substitution level of $x = 0.10$. Conversely, the peak identified as $VL$ (*006*) is noted to appear immediately after the substitution level of $x = 0.05$ at $2\theta$ of $\sim$ 21.88° when the other peak of $VL$ (*00*$\underline{12}$) emerged at $2\theta \sim$ 43.62° is observed in the XRD diffractograms. Moreover, no observation of diffraction peaks related to any cationic phase of $Ho_2O_3$ compound presents that the solubility limit level for the holmium impurities is not determined in the Bi-2212 matrix [42, 43].

Further, the role of trivalent Ho/Bi partial replacement on the lattice cell parameters of Bi-2212 superconducting system is investigated by the shifts of $2\theta$ angles towards to high/low angles. It is obvious from Fig. 1 that the positions of characteristic diffraction peaks including $H$ (*002*), $L$ (*002*), $L$ (*008*), $H$ (*00*$\underline{10}$), $L$ (*00*$\underline{10}$), $H$ (*00*$\underline{12}$), and $L$ (*00*$\underline{12}$) are found to shift to the small-2θ angles in case of the optimum Ho/Bi substitution level of $x = 0.01$ after which all the peaks are observed to shift towards to the large-$2\theta$ angles depending on the variation of $c$-axis length in the crystal structure. For the characteristic peak of $H$ (*020*), the peak initially shifts to large-angle values and then to the small-angle region. This is attributed to the fact that for the tetragonal crystal structure ($a$ is equal to $b$), the $c$-axis length presents the opposite relation to the $a$ and $b$ lattice constants. All the cell parameters of pure and Ho/Bi partial-substituted Bi-2212 superconductors are calculated for the tetragonal unit cell structure with space group $P_{4/mmm}$ by means of the formulation of $\frac{1}{d^2} = (\frac{h^2}{a^2} + \frac{k^2}{b^2} + \frac{l^2}{c^2})$, where $d$ shows the lattice spacing and (*hkl*) indicates the diffraction planes. One can see all the computations in Table 1. It is apparent from the table that the $c$-axis length is determined as about 30.66 Å when the lattice cell parameter is found to be about 5.36 Å. In case of the optimum substitution level, the $a$ cell constant is detected to reduce to the smallest value of 5.32 Å and $c$-axis length is found to enlarge to the global maximum value of 32.55 Å. However, after the critical substitution level of $x = 0.01$, the systems turns conversely. On this basis, the $a$ cell parameter begins to climb towards to the largest value of about 5.44 Å whereas the $c$-axis length gets smaller and smaller and reaches to the lowest value of 30.14 Å for the highest substitution level of $x = 0.10$. The influence of

homovalent Ho/Bi partial replacement can be summarized as below: initially the superconducting nature improves with the optimum Ho/Bi substitution as a consequence of the positive effect on the formation of thermodynamically activated super-electrons and mobile hole carrier concentration per Cu ions in the valance bands. The basal plane sizes and electrons into the anti-bonding orbitals decrease with optimum substitution and accordingly the interlayer spaces of Cu–Ca–Cu and Ca–Sr sites contract to balance the changes [44–46]. Besides, the elongation of *c*-axis length results from the charge neutrality mechanism related to the balance of oxygen level in the Bi–O double layers [47]. In this respect, the effective layers in the Bi-2212 superconducting matrix and corresponding interlayer spaces of Sr–Bi, Bi–Bi and Sr–Bi–Bi–Sr sites enlarge depending on the increment in the *c*-axis length [48]. Moreover, maybe different electron configuration of outer shells can explain the variation of *c* lattice cell constant with the trivalent Ho/Bi partial replacement in the Bi-2212 crystal structure. In more detail, the Bi atoms with the outer atomic electron configuration of $6s^2 6p^3$ are totally different than that of $4f^{11} 6s^2$ for Ho atoms. When encountering the valencies of Bi–O layers in the polycrystallized Bi-2212 superconductor, the atom integrates with the surrounding oxygen atoms. Based on the information, it is to be mentioned here that the $Ho^{+3}$ ions are much easier integrated by the surrounding valencies of Bi–O layers with the formation of fsp orbital hybrid since the integration is only bond of p–p for the $Bi^{+3}$ ions [49]. In the optimum substitution level, the integration of $Ho^{+3}$ ions consumes much less energy for the formation of bonds, leading to form thermodynamically activated super-electrons in the homogeneous superconducting cluster percentages in the paths. On the other hand, in case of excess $Ho^{+3}$ ions in the crystal system, the extra energy is required for the formation of bonds and super-electrons. This information explains why the Bi-2223 and Bi-2212 superconducting phases degrade with the excess dopant.

The variation of average crystallite sizes over the trivalent Ho/Bi partial replacement is also examined from the diffraction patterns of materials using Scherrer equation approach that is grounded on the full width at half maximum for the peaks [50]. Namely,

$$t = K\lambda / B\cos\theta B, \tag{4}$$

in the equation $t$ shows the mean crystallite/grain size when $\lambda$ indicates the wavelength of incident X-rays. The constant of K depends on the crystal geometry and distribution of sizes. According to the crystal thickness grown in the current work, K is estimated to be about 0.941 and used to determine the mean crystallite size parameters of materials produced in this work. The abbreviation of $\theta_B$ is related to Bragg angle when $B$ reveals the full width at half maximum of Bragg peak. All the computation data are numerically depicted in Table 1. It is visible from the table that the pure sample possesses 58 nm average crystallite size while the Ho/Bi-1 (best) sample obtains the maximum average crystallite size of 60 nm. After the critic replacement level of x = 0.01, the grain size gets smaller and smaller and reaches to the global minimum value of 51 nm. The results clearly show that the optimum Ho/Bi substitution favors the growth of average crystallite size of Bi-2212 superconducting system. In other words, the presence of optimum holmium atoms in the system improves the crystallinity and strength quality of connectivity between the grains. Conversely, the excess Ho particles cause to increase the serious crystallinity problems in the Bi-2212 superconducting system.

The experimental XRD patterns enable to calculate Lotgering index ($F$) related to the alignments of crystallographic diffraction planes in the powders. In other words, the parameter is used to quantify the *c*-axis orientation degrees of diffraction peaks in the polycrystalline superconducting $Bi_{2.1-x}Ho_xSr_{2.0}Ca_{1.1}Cu_{2.0}O_y$ ceramic compounds [51, 52]. According to Fig. 1, the plane reflection intensities generally result from *00 l* diffraction planes depending on the arrangement in the crystal plane alignments towards to the c-axis orientation as a consequence of plate-like structure. One can see the variation in the *c*-axis orientation degrees of diffraction peaks on the homovalent Ho/Bi partial substitution level in Table 1. It is apparent from the table that the pure sample exhibits the Lotgering index value of 0.44 while the Ho/Bi-1 superconductor possesses the maximum value of 0.49. After the critic Ho/Bi dopant level of $x = 0.01$, the index value is observed to decrease considerably depending on the replacement value. In this context, the Lotgering index falls into the deepest value of 0.37 for the Ho/Bi-5 sample. This means that in case of the optimum trivalent Ho/Bi

substitution level, the *c*-axis orientation degrees and texturing of superconducting grain couplings improve remarkably. Conversely, the presence of excess holmium ions in the Bi-2212 superconducting crystal structure damages seriously the grain alignment distributions and orientations.

### 4.2 Relative residual porosities based on bulk density measurements

As well known, the bulk density experiments are widely used to determine the crystallinity problems (microscopic cracks, impurity residues, porosity, microvoid/grain coalescences, impurity residues, grain alignment distributions/orientations, internal and structural omnipresent defects), strength quality of intra and inter-grain boundary couplings and capability of flux pinning mechanisms in the crystal structure whether the material can be preferred in the usage of advanced engineering, heavy-industrial technology, and large-scale application fields, or not [53]. Hence, the bulk density is received to be directly related to the degree of granularity or sometimes called as the residual porosity [54]. In this respect, there are several methods to determine the bulk density of a material. Among the available techniques, Archimedes water displacement experiment with some advantages such as low-cost, fast, simple, and reliable features is one of the most preferred submethods to define the bulk density and derived residual porosity (degree of granularity) parameter. In the current work, the variation of bulk density and residual porosity parameters with the homovalent Ho/Bi partial replacement level in the bulk $Bi_{2.1-x}Ho_xSr_{2.0}Ca_{1.1}Cu_{2.0}O_y$ $(0 \leq x \leq 0.1)$ superconducting ceramic compounds is meticulously carried out by the standard Archimedes water displacement experiments. One can numerically see that all the experimental test results findings in Table 2. It is apparent from the table that there are different bulk density values depending on the substitution level. This is in association with the fact that the trivalent $Ho^{3+}$ atoms are successfully replaced by the $Bi^{3+}$ impurities in the Bi-sites of Bi-2212 superconducting crystal system. Numerically, the pure sample presents the moderate value of 5.89 g/cm$^3$ when the bulk density parameter is found to be the highest value of 6.04 g/cm$^3$ for the bulk Ho/Bi-1 (best) material. Conversely, the parameter tends to degrade systematically with the cationic substitution of trivalent Ho/Bi in the Bi-2212 crystal system. On this basis, the smallest value of 5.71 g/cm$^3$ is recorded for the polycrystallized Ho/Bi-5 (worst) superconductor. It is obvious that the inner (Ho/Bi-1) sample exhibits the densest with the combination of lowest porous and largest particle distributions well linked each other whereas the latter (Ho/Bi-5) compound shows the most granular structure with new induced crystallinity problems and especially decrement in the strength quality of intra- and inter-grain boundary couplings in the crystal structure. All in all, the excess holmium concentration is principal responsible for the diminish of bulk density. Regardless, it is to be mentioned here that the existence of optimum Ho impurity content in the Bi-2212 crystal system strengthens the crystallinity quality and strength quality of intra- and inter-grain boundary couplings.

At the same time, with the use of bulk density findings, the differentiation in the degree of granularity parameters with the trivalent Ho/Bi partial substitution is determined. The calculations are performed according to the density of 6.30 g/cm$^3$ for the pure Bi-2212 system [55] as depicted in Ref. [56, 57]. One can see the effect of holmium concentration on

**Table 2** Dc electrical resistivity measurement results including $\rho_{300K}$, $\rho_{res}$, $\rho_{90K}$, $\rho_{norm}$, $\Delta\rho$, and *RRR* for all the materials studied in this work. $P_{hole}$ and *RRR* parameters and Archimedes water displacement findings as regards $\rho$ and $P$

| Materials | $\rho_{300K}$ (mΩcm) | $\rho_{res}$ (mΩcm) | $\rho_{90K}$ (mΩcm) | $\Delta\ \rho$ ($\rho_{300K}$—$\rho_{90K}$) (mΩcm) | $\rho_{norm}$ ($\rho_{90}/\Delta\ \rho$) | RRR ($\rho_{300K}/\rho_{90K}$) |
|---|---|---|---|---|---|---|
| Pure | 5.08 | 1.32 | 2.49 | 2.59 | 0.96 | 2.04 |
| Ho/Bi-1 | 3.91 | 0.64 | 1.52 | 2.39 | 0.64 | 2.57 |
| Ho/Bi-2 | 5.40 | 2.93 | 3.71 | 1.69 | 2.20 | 1.46 |
| Ho/Bi-3 | 7.74 | 4.55 | 5.46 | 2.28 | 2.40 | 1.42 |
| Ho/Bi-4 | 9.95 | 6.61 | 7.55 | 2.40 | 3.15 | 1.32 |
| Ho/Bi-5 | 11.76 | 8.80 | 9.71 | 2.05 | 4.74 | 1.21 |

the residual porosities of oxygen-deficit multi-layered perovskite-based $Bi_{2.1-x}Ho_xSr_{2.0}Ca_{1.1}Cu_{2.0}O_y$ superconducting ceramic compounds in Table 2. It is apparent from the table that the relative degree of granularity parameter is found to be about 6.51% for the pure sample as against 4.13% for the best (Ho/Bi-1) compound. After the critical substitution level of $x = 0.01$, the residual porosity parameter tends to increase immediately and reaches to the maximum value of 9.37% for the worst (Ho/Bi-5) sample. This means that the excess (optimum) Ho/Bi substitution level supports (decreases) the granular structure of host Bi-2212 superconducting crystal system due to the increment in the crystallinity and related structural problems.

### 4.3 Dc electrical resistivity findings of $Bi_{2.1-x}Ho_xSr_{2.0}Ca_{1.1}Cu_{2.0}O_y$ superconducting systems

The influence of homovalent Ho/Bi partial substitution in the oxygen-deficit multi-layered perovskite-based $Bi_{2.1-x}Ho_xSr_{2.0}Ca_{1.1}Cu_{2.0}O_y$ superconducting ceramic compounds on the dc electrical resistivity features is determined by means of temperature-dependent electrical resistivity measurements in the temperature range of 15 K–101 K as given in Fig. 2. The dc electrical resistivity curves enable us to find the basic electrical and superconducting parameters such as dc electrical resistivity at room temperature ($\rho_{300K}$), residual resistivities ($\rho_{res}$), residual resistivity ratios ($RRR$), $\rho_{90K}$, $\rho_{norm}$, $\Delta\rho$, offset $Tc^{offset}$ and onset

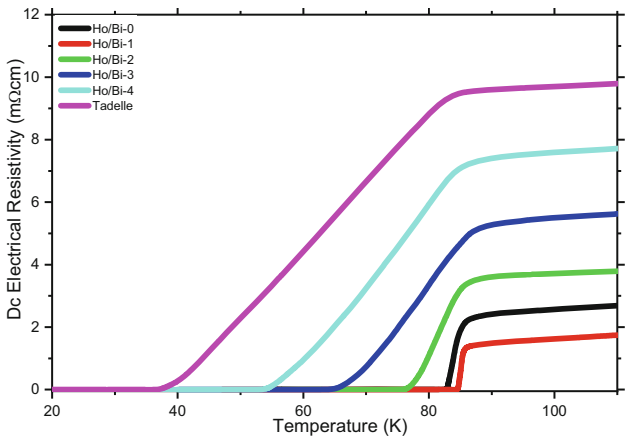


**Fig. 2** Dc electrical resistivity results versus temperatures between 35 and 105 K for oxygen-deficit multi-layered perovskite-based $Bi_{2.1-x}Ho_xSr_{2.0}Ca_{1.1}Cu_{2.0}O_y$ superconducting ceramic compounds

$Tc^{onset}$ critical transition temperatures, and degree of broadening $\Delta Tc = Tc^{offset} - Tc^{onset}$ parameters. Prior to the crucial experimental findings, it is obvious from the experimental curves in Fig. 2 that the Ho/Bi substitution level clearly affects the electrical characteristic behaviors. This means that the trivalent $Ho^{3+}$ cationic impurities are successfully replaced for the $Bi^{3+}$ cations in the Bi-2212 superconducting matrix. Besides, the curves indicate that the pure and Ho/Bi partial-substituted Bi-2212 superconducting materials exhibit the truly metallic transition nature with the positive linear dependence ($d\rho/dt$) of electrical resistivity versus temperature after their own $T_c^{onset}$ values. Shortly, the behavior stems from the logarithmic distribution of densities of active and effective electronic states (DOS) at the vicinity of Fermi level [58–60]. Similarly, the $d\rho/dt$ behavior is related to the strong interactions between electron–phonon in the homogeneous superconducting cluster percentages in the paths causing the formation of cooper-pair probabilities and superconducting phenomenon [61, 62]. Especially, in case of the optimum substitution level of $x = 0.01$, the Bi-2212 superconducting material presents the best metallic character as a result of the improvement in the metallic interactions between the intra- and inter-grain region and mobile hole carrier concentration per Cu ions in the valance bands, to be discussed in more detail in the following parts [63]. It is, of course that the crystallinity quality is notably refined with the optimum holmium content in the crystal system and much more superconducting grains are coupled to each other, as provided in the previous sections. Conversely, the excess holmium ions damage the metallic interactions between the intra- and inter-grain region because of new induced permanent crystallinity problems [64–66].

The dc electrical resistivity curves enable us to examine the effect of Ho/Bi partial replacement on the room temperature and 90 K resistivity parameters ($\rho_{300K}$ and $\rho_{90K}$ parameters) of bulk $Bi_{2.1-x}Ho_xSr_{2.0}Ca_{1.1}Cu_{2.0}O_y$ superconducting ceramic compounds. It is found that both the parameters present the similar changing trends (initially decrease for $x = 0.01$ substitution level and then rapid increment). In this respect, the $\rho_{300K}$ ($\rho_{90K}$) parameter is recorded to reduce remarkably from the value of about 5.08 mΩ cm (2.49 mΩ cm) for the pure compound until 3.91 mΩ cm (1.52 mΩ cm) for the Ho/Bi-

1 sample as a consequence of the refinement in the crystallinity quality and strength quality of intra- and inter-grain boundary couplings in the bulk Bi-2212 superconducting materials. Especially, the decrement in the $\rho_{90K}$ parameter related to the phase transition between the superconducting and normal state for the interior of isolated grains along the transcrystalline regions indicates that the presence of optimum holmium impurities in the Bi-2212 crystal lattice eliminates the impurity scattering mechanism and formation of lattice strains in the Bi-2212 crystal system [67]. However, after the certain substitution level of $x = 0.01$, both the parameters are observed to enhance harshly due to the deterioration in the crystallinity qualities depending on the increment in the grain boundary coupling problems and interaction between the superconducting grains, being already confirmed by the other parts. On this basis, the bulk Ho/Bi-5 sample possesses the highest $\rho_{300K}$ and $\rho_{90K}$ values of 11.76 mΩ cm and 9.71 mΩ cm, respectively (Table 2).

Moreover, the pure and Ho/Bi partial-replaced Bi-2212 superconductors exhibit the similar trend for the residual resistivity parameter inferred from Matthiessen's rule [68]. On this basis, the smallest $\rho_{res}$ parameter of 0.64 mΩ cm is measured for the Ho/Bi-1 superconducting ceramic compound whereas the polycrystallized Ho/Bi5 compound has the highest $\rho_{res}$ parameter of 8.80 mΩ cm. The other samples (pure, Ho/Bi-2, Ho/Bi-3, and Ho/Bi-4) exhibit the moderate values between 1.32 mΩ cm (for the pure sample) and 6.61 mΩ cm (for the Ho/Bi-4 sample). The chance of $\rho_{res}$ parameter is another observation to confirm the dependence of crystal quality belonging to the Bi-2212 superconducting system on the trivalent Ho/Bi partial substitution (Table 3).

Furthermore, the direct ratio between $\rho_{90K}$ and $\rho_{300K}$ is used to define the residual resistivity ratio ($RRR = \rho_{300K}/\rho_{90K}$) of the superconducting materials and determine the material quality qualification for the suitability of usage in the advanced engineering, heavy-industrial technology, and large-scale application fields [69]. One can see the change of RRR parameters of bulk $Bi_{2.1-x}Ho_xSr_{2.0}Ca_{1.1}Cu_{2.0}O_y$ superconducting ceramic compounds with the homovalent Ho/Bi partial replacement in Table 2 in detail. It is observed from the table that the *RRR* parameter depends sensitively on the substitution level. In this context, the pure sample exhibits the *RRR* value of 2.04 (relatively higher) while the Ho/Bi-1 sample has the maximum value of 2.57. On the other hand, beyond the critical replacement value of $x = 0.01$, the *RRR* parameter begins to reduce and in fact crashes to the deepest value of 1.21 for the Ho/Bi-5 material. It is clear from the table that both the pure and especially Ho/Bi-1 sample possess the appropriate material quality for application areas. It seems that the optimum homovalent substitution of $Ho^{3+}$ ions for the $Bi^{3+}$ ions in the crystal system enables the bulk Bi-2212 superconducting materials to find much more application fields. However, the existence of excess holmium content obviously damages the sample quality and intra- and inter-grain boundary couplings.

Additionally, the differentiation between $\rho_{300K}$ and $\rho_{90K}$ parameter ($\Delta\rho = \rho_{300K}-\rho_{90K}$: auxiliary parameter) is used to describe the $\rho_{norm}$ parameter so that we can define the structural disorders, crystallinity problems, and defects in the crystal system. In the current study, we search the role of homovalent Ho/Bi partial substitution in the Bi-2212 superconducting materials on the structural disorders and defects in the crystal system. First of all, we calculate the $\Delta\rho$ parameters for ever material and depict numerically in Table 2. It is apparent from the table that the $\Delta\rho$ values are not found in any particular order. To illustrate, the pure sample has 2.59 mΩ cm followed by a decrement towards to 2.39 mΩ cm and 1.69 mΩ cm for the Ho/Bi-1 and Ho/Bi-2 samples, respectively. The parameter tends to increase again to

**Table 3** Superconducting temperature quantities of $T_c^{onset}$, $T_c^{offset}$ and $\Delta T_c$, $P_{hole}$, and Archimedes water displacement findings of $\rho$ and $P$

| Samples | $T_c^{offset}$ (K) | $T_c^{onset}$ (K) | $\Delta T_c$ (K) | $P_{hole}$ | $\rho$ (g/cm$^3$) | $P$ (%) |
|---|---|---|---|---|---|---|
| Pure | 82.12 | 84.61 | 2.49 | 0.14 | 5.89 | 6.51 |
| Ho/Bi-1 | 84.26 | 84.96 | 0.68 | 0.15 | 6.04 | 4.13 |
| Ho/Bi-2 | 75.21 | 83.12 | 7.91 | 0.12 | 5.82 | 7.62 |
| Ho/Bi-3 | 62.01 | 82.54 | 20.53 | 0.10 | 5.78 | 8.25 |
| Ho/Bi-4 | 52.96 | 82.13 | 29.17 | 0.09 | 5.74 | 8.89 |
| Ho/Bi-5 | 34.13 | 78.07 | 43.94 | 0.07 | 5.71 | 9.37 |

2.28 mΩ cm and 2.40 mΩ cm for the Ho/Bi-3 and Ho/Bi-4 compounds as against 2.05 mΩcm for the bulk Ho/Bi-5 superconductor. If passing the main characteristic parameter using the formula of $\rho_{norm} = \rho_{90K}/\Delta\rho$ (ratio between the $\rho_{90}$ and $\Delta\rho$ parameters), we can easily observe the change in the structural disorders, crystallinity problems, and defects in the Bi-2212 crystal system with the Ho/Bi partial substitution [70, 71]. One can see all the $\rho_{norm}$ parameters in Table 2. It is obvious from the table that the lowest parameter of 0.64 is reported for the best (Ho/Bi-1) compound whereas the maximum value of 4.74 is detected for the bulk Ho/Bi-5 sample. It is to be mentioned here that a very sharp enhancement is observed after the partial substitution level of $x = 0.03$. According to the results, it can easily be revealed that the optimum trivalent Ho/Bi substitution improves considerably the crystallinity quality of perovskite-based Bi-2212 crystal structure while the excess $Ho^{3+}$dopant results in the formation of new structural disorders, crystallinity problems, and defects in the bulk Bi-2212 superconducting materials, being already verified by the other sections of paper.

It is another important result that the combination of dc electrical resistivity and XRD patterns shows that there is a closer relationship between the fundamental electrical features and Bi-2223 phase. Thus, it is anticipated that the formation of Bi-2223 phase in the polycrystallized Bi-2212 superconducting system positively affects the electrical characteristics quantities.

### 4.4 Influence of trivalent Ho/Bi substitution on superconducting nature of Bi-2212 ceramics

The dc electrical resistivity curves are also used to determine the superconducting temperature quantities (parameters of $T_c^{onset}$, $T_c^{offset}$, and $\Delta T_c$) of oxygen-deficit multi-layered perovskite-based $Bi_{2.1-x}Ho_xSr_{2.0}Ca_{1.1}Cu_{2.0}O_y$ superconducting ceramic compounds. Basically, $T_c^{offset}$ is directly related to the phase transition of intragrain and inter-granular components into the superconducting phase [72] and defined as the temperature that begins to form the effective electron–phonon coupling probabilities (super-electrons) in the homogeneous superconducting cluster percentages in the paths [73]. As for $T_c^{onset}$ parameter, the transcrystalline regions become superconductive below the temperature value, and thus, the parameter is used to determine the presence of hybridization mechanism in the system, order parameter belonging to the super-electrons, clean/dirty limit characteristics, metastability, localization of DOS in the long-range ordered state, overlapping mechanism for the Cu-3d and O-2p wave functions, formation of thermodynamically activated super-electrons, and mobile hole carrier concentration per Cu ions in the valance bands [74]. On this basis, we investigate the effect of homovalent Ho/Bi partial replacement on the $T_c^{offset}$ and $T_c^{onset}$ parameters by means of dc electrical resistivity measurements performed in the temperature range from 35 to 105 K. Besides, the degree of broadening parameter ($\Delta T_c$) for every compound studied in the present work is deduced from the subtraction of $T_c^{onset}$–$T_c^{offset}$. One can see all the computations related to the $T_c^{onset}$, $T_c^{offset}$, and $\Delta T_c$ parameters in Table 2. It is apparent from the table that the parameters every are found to be strongly dependent upon the trivalent Ho/Bi concentration level. Accordingly, while the pure sample possesses the $T_c^{onset}$ and $T_c^{offset}$ values of 84.61 K and 82.12 K, the Ho/Bi-1 sample with the best crystallinity quality exhibits the highest $T_c^{onset}$(84.96 K) and $T_c^{offset}$ values (84.26 K). However, with the increment in the substitution level, the parameters (especially offset one) are recorded to reduce dramatically. In this respect, the Ho/Bi-5 sample with the highest grain boundary coupling problems possesses the minimum values of 78.07 K and 34.13 K for the $T_c^{onset}$ and $T_c^{offset}$ values, respectively. The dramatic reduction of parameters results from the induced inhomogeneities in the oxidation state of superconducting grains and decreased DOS at Fermi energy level. To sum up, the presence of optimum $Ho^{3+}$ ions in the Bi-2212 superconducting matrix favors the formation of thermodynamically activated super-electrons in the homogeneous superconducting cluster percentages in the paths and mobile hole carrier concentration in the valance bands while the excess replacement harms significantly the phase transition of intragrain and particularly inter-granular components, leading both to disappear the super-electrons in the bulk Bi-2212 crystal structure and to diverge from the mobile hole carrier concentration per Cu ions in the valance bands. Similarly, the induced permanent crystallinity

problems with the excess substitution level damage seriously the fundamental superconducting parameters. The increment in the crystallinity problem with the excess substitution level is also confirmed by the experimental and theoretical results of powder X-ray diffraction (XRD) investigations. In more detail, the experimental results and theoretical approaches show that there seems a perfect accordance between the electrical/superconducting properties and crystallinity mechanisms depending on the Ho/Bi partial substitution level. Hence, the optimum trivalent Ho/Bi replacement is a good preference to increase in the usage of multi-layered perovskite-based $Bi_{2.1-x}Ho_xSr_{2.0}Ca_{1.1}Cu_{2.0}O_y$ superconducting materials in the critical application fields.

As for the differentiation of $\Delta T_c$ parameters with the partial cationic replacement level, among the materials, the Ho/Bi-1 sample presents the smallest value of 0.68 K whereas the maximum parameter of 43.94 K is observed for the Ho/Bi-5 sample as expected. The other samples obtain the moderate values between 7.91 K and 29.17 K. The rapid decrement explains clearly the presence of strong relationship between the crystallinity quality and $\Delta T_c$ parameter.

Additionally, the variation of mobile hole carrier concentration per Cu ions in the valance bands for the Bi-2212 crystal structure with the trivalent Ho/Bi partial cationic substitution using the following equation [75]:

$$P = 0.16 - \left[\left(1 - \frac{Tc^{\text{onset}}}{Tc^{\text{max}}}\right)/82.6\right]^{1/2}, \quad (5)$$

where $T_c^{\text{max}}$ is 85 K for the Bi-2212 superconducting phase and the $T_c^{\text{offset}}$ values are taken form data in Table 2. One can see all the numerical calculations in Table 2. It is apparent from the table that the increase in the holmium ions affects seriously the $P_{\text{hole}}$ parameter. The pure sample has the $P_{\text{hole}}$ value of 0.13975 while the Ho/Bi-1 sample possesses the maximum value of 0.14973 followed by the rapid degradation toward to 0.07488 with the increase in the cationic substitution level. To illustrate in more detail, we draw a plot including the mobile hole carrier concentration versus Ho/Bi substitution level as given in Fig. 3. According to the figure, from the critical substitution level of $x = 0.01$ onwards, the mobile hole carrier concentration parameters harshly diverge from the optimum value and in fact are dramatically damaged with the increment trend in the cationic replacement concentration level (Fig. 3).

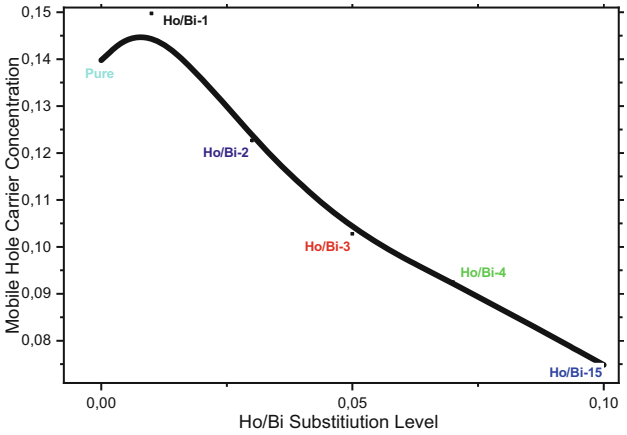


**Fig. 3** Differentiation of mobile hole carrier concentration per Cu ions in the valance bands as a function of Ho/Bi substitution level

## 4.5 Relationships between fundamental characteristic quantities

In this part of paper, we develop the strong links between fundamental characteristic quantities (powder X-ray diffraction, bulk density, dc electrical resistivity versus temperature) depending on the homovalent Ho/Bi partial replacement in the crystal system. On this basis, the changes in the electrical resistivity quantities ($\rho_{300K}$, $\rho_{res}$, $RRR$, $\rho_{90K}$ and $\rho_{norm}$) related to the quality factors with respect to the experimental bulk densities in Fig. 4a. It is apparent from the figure that all the electrical quantities (except for the RRR values with the reverse dependence as expected) move parallel with the bulk density values. Here, there is a critic substitution point of $x = 0.03$ after which all the parameters change rapidly due to the crucial deterioration in the crystallinity quality and strength quality of intra- and inter-grain boundary couplings in the bulk Bi-2212 superconducting materials. On this basis, the experimental bulk density value corresponding to the degradation is about 5.8 g/cm$^3$.

Similarly, we depict the variation of $c$-axis length and average crystallite size (deduced from the diffraction peaks in the XRD diffractograms) as a function of the experimental bulk density parameters in Fig. 4b. It is apparent form the figure that both the parameters of $c$-axis length and average crystallite size tend to enlarge with the increase in the bulk density parameters (especially after the point of

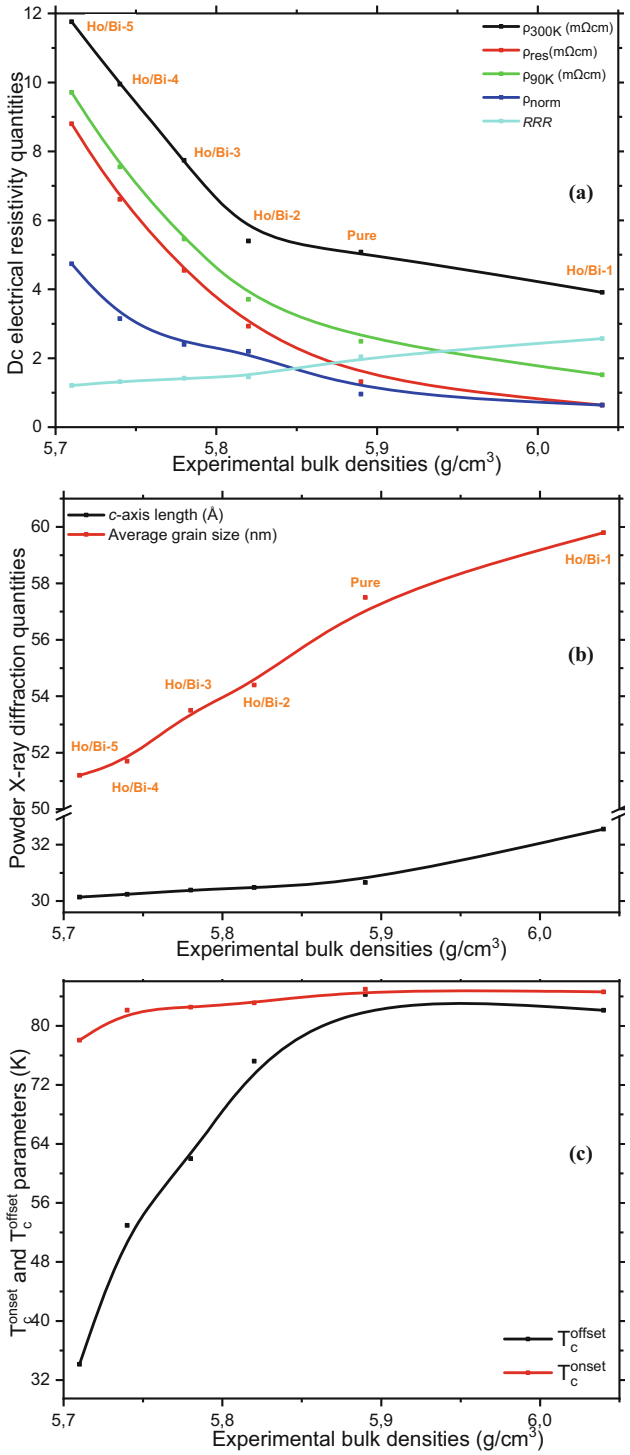


**Fig. 4** Variation in fundamental characteristic quantities over experimental bulk densities: **a** electrical resistivity quantities ($\rho_{300K}$, $\rho_{res}$, $RRR$, $\rho_{90K}$ and $\rho_{norm}$), **b** $c$-axis length and average crystallite size, and **c** $T_c^{onset}$ and $T_c^{offset}$ values

about 5.8 g/cm$^3$). This is attributed to the fact that the increased dense character (with much more isolated grains throughout the transcrystalline regions) for the bulk Bi-2212 crystal system supports extensively the formation of thermodynamically activated super-electrons in the homogeneous superconducting cluster percentages in the paths and mobile hole carrier concentration per Cu ions in the valance bands.

Moreover, to examine the change of $T_c^{onset}$ and $T_c^{offset}$ values over the experimental bulk density parameters, we plot the data in Fig. 4c. Similar to the other findings, the figure shows that both the parameters (particularly $T_c^{offset}$ ones) diminish rapidly before the bulk density parameter value of about 5.8 g/cm$^3$. In this respect, the increment in the granular structure based on the experimental bulk density truncates the fundamental superconducting formation mechanisms. To sum up, all the experimental findings and theoretical results are found to be perfect agreement with each other.

## 5 Conclusion

The part establishes a strong conclusion grounded on the role of homovalent Ho/Bi partial substitution on the fundamental characteristic features including the dc electrical resistivity, superconducting, bulk density, general crystallinity qualities, degree of granularity, strength quality of intra- and inter-grain boundary couplings in the polycrystalline Bi-2212 ceramic compounds prepared by the standard solid-state reaction method within the mole-to-mole ratio intervals $0.00 \leq x \leq 0.30$. The characterization of ceramics is extensively carried out by means of conventional identification experimental methods, namely, powder X-ray diffraction, temperature-dependent electrical resistivity, and Archimedes water displacement techniques.

Based on the experimental and theoretical results, the trivalent $Ho^{3+}$ impurities are successfully substituted for the $Bi^{3+}$ particles in the Bi-2212 crystal system, and the optimum concentration is noted to be $x = 0.01$ for the bulk superconducting ceramics. In this respect, the main conclusions possessed are provided as follows:

- Diffraction patterns in the XRD diffractograms indicate that there seem serious changes (new appearance, disappearances of shift) in the two-theta angles and intensities of diffraction peaks. In

this respect, the experimental and theoretical calculation results display that the presence of optimum holmium in the Bi-2212 superconducting crystal lattice improves the formation velocity of high Bi-2223 superconducting phase towards to the volume fraction value of 33.48%; however, after the critical replacement value of $x = 0.01$, the high phase begins to reduce immediately and reaches to the global minimum point of 4.13%. Similarly, the bulk Ho/Bi-1 sample possesses the largest *c*-axis length of 32.55 Å and smallest *a* lattice cell constant of 5.32 Å. Besides, the optimum Ho impurity affects positively the average crystallite size (60 nm) and Lotgering index (0.487) parameters. They are just those last descriptors that are the remarkable improvement in the *c*-axis orientation degrees, texturing of superconducting grains, and strength quality of intra- and inter-grain boundary couplings in the bulk Bi-2212 superconducting materials.

- The bulk density experimental results also reveal that the presence of optimum holmium atoms in the Bi-2212 crystal structure augments the density of material due to the decrement in the porosity depending on the granular nature of Bi-2212 superconductor. Accordingly, the Ho/Bi-1 compound presents the highest bulk density value of 6.04 g/cm$^3$ with the smallest residual porosity parameter of 4.13%. On the other hand, the excess holmium damages the density of material and results in the increment the degree of granularity parameter towards to 9.37%.
- Furthermore, the $\rho$-T experiment results present that the optimum homovalent Ho/Bi partial substitution in the Bi-2212 superconducting matrix favors the formation of thermodynamically activated super-electrons in the homogeneous superconducting cluster percentages in the paths and mobile hole carrier concentration in the valance bands. Likewise, the homogeneities in the oxidation state of superconducting grains and the number of DOS at Fermi energy level enhance dramatically in case of the optimum substitution level. As for the excess holmium concentration, the phase transitions of intragrain and particularly inter-granular components are damaged.
- The samples substitutions with Ho exhibit the best crystallinity quality, grain alignment distributions/orientations, and highest strength quality of intra- and inter-grain boundary couplings in the crystal structure, being already verified by bulk density experimental results.

All in all, the experimental measurement results and calculations indicate that the fundamental characteristic features are observed to improve considerably in case of the optimum homovalent Ho/Bi partial replacement in the oxygen-deficit multi-layered perovskite-based $Bi_{2.1}Sr_{2.0}Ca_{1.1}Cu_{2.0}O_y$ ceramic compounds. Accordingly, this study proposes that the optimum substitution enables the Bi-2212 superconducting materials to find easily application fields in the novel and feasible market areas for the universe economy.

## Acknowledgements

The authors would like to express their gratitude to Kırıkkale University Research Fund for its financial support. Project Number: 2020/038.

## Declarations

**Conflict of interest** The author declares that there are no known competing financial interests or personal relationships that could have appeared to influence the work reported in this paper.

## References

1. H.K. Onnes, Further experiments with Liquid Helium. D On the change of electrical resistance of pure metals at very low Temperatures, etc. V. The disappearance of the resistance of mercury. Koninklijke Nederlandsche Akademie van Wetenschappen Proc. **14**, 113–115 (1911)
2. S.B. Guner, Y. Zalaoglu, T. Turgay, O. Ozyurt, A.T. Ulgen, M. Dogruer, G. Yildirim, A detailed research for determination of Bi/Ga partial substitution effect in Bi-2212 superconducting matrix on crucial characteristic features. J. Alloys Compd. **772**, 388–398 (2019). https://doi.org/10.1016/j.jallcom.2018.09.071
3. B. Akkurt, U. Erdem, Y. Zalaoglu et al., Evaluation of crystallographic and electrical-superconducting features of Bi-2223 advanced ceramics with vanadium addition. J. Mater. Sci. **32**, 5035–5049 (2021). https://doi.org/10.1007/s10854-021-05238-5
4. A.T. Ulgen, T. Turgay, C. Terzioglu, G. Yildirim, M. Oz, Role of Bi/Tm substitution in Bi-2212 system on crystal structure

quality, pair wave function and polaronic states. J. Alloys Compd. **764**, 755–766 (2018)
5. I.A. Parinov, *Microstructure and Properties of High-Temperature Superconductors* (Springer, Berlin, 2007)
6. V.L. Ginzburg, E.A. Andryushin, Superconductivity, Revised ed. World Scientific Pub. Co. Inc. (2004).
7. M. Pakdil, E. Bekiroglu, M. Oz, N.K. Saritekin, G. Yildirim, Role of preparation conditions of Bi-2223 ceramic materials and optimization of Bi-2223 phase in bulk materials with experimental and statistical approaches. J. Alloys Compd. **673**, 205–214 (2016)
8. G. Yildirim, Determination of optimum diffusion annealing temperature for Au surface-layered Bi-2212 ceramics and dependence of transition temperatures on disorders. J. Alloys Compd. **699**, 247–255 (2017)
9. W. Buckel, R. Kleiner, *Superconductivity: Fundamentals and Applications*, 2nd edn. (Wiley, Weinheim, 2004)
10. F.N. Werfel, U. Floegel-Delor, R. Rothfeld, T. Riedel, B. Goebel, D. Wippich, P. Schirrmeister, Superconductor bearings, flywheels and transportation. Supercond. Sci. Technol. **25**, 014007 (2012)
11. M. Runde, Application of high-$T_c$ superconductors in aluminum electrolysis plants. IEEE T. Appl. Supercond. **5**, 813–816 (1995)
12. S.Y. Oh, H.R. Kim, Y.H. Jeong, O.B. Hyun, C.J. Kim, Joining of Bi-2212 high-$T_c$ superconductors and metals using indium solders. Physica C **463–465**, 464–467 (2007)
13. U. Erdem, Y. Zalaoglu, A.T. Ulgen, T. Turgay, G. Yildirim, Role of trivalent Bi /Tm partial substitution on active operable slip systems in Bi 2212 crystal structure. Cryogenics **113**, 103212 (2021)
14. H. Yamauchi, M. Karppinen, Application of high-pressure techniques: stabilization and oxidation-state control of novel superconductive and related multi-layered copper oxides. Supercond. Sci. Techol. **13**, R33–R52 (2000)
15. M.E. Takayama, High-pressure synthesis of homologous series of high critical temperature ($T_c$) superconductors. Chem. Mater. **10**, 2686–2698 (1998)
16. A.T. Ulgen, G. Yildirim, Gece Kitapligi, Change in Key Mechanical Design Quantities of Bi-2212 Superconducting System with Various Annealing Ambient, pp. 331–349, Ankara
17. Hartinger, C. DFG FG 538 – Doping Dependence of Phase transitions and Ordering Phenomena in Cuprate Superconductors.
18. H. Hilgenkamp, J. Mannhart, Grain boundaries in high $T_c$ superconductors. J. Rev. Mod. Phys. **74**, 485–549 (2002)
19. C. Autret-Lambert, B. Pignon, M. Gervais, I. Monot-Laffez, A. Ruyter, L. Ammor, F. Gervais, J.M. Bassat, R. Decourt, Microstructural and transport properties in substituted $Bi_2Sr_2CaCu_2O_{8+delta}$ modulated compounds. J. Solid State Chem. **179**, 1698–1706 (2006)
20. K. Salama, V. Selymanickam, L. Gao, K. Sun, High-current Density in Bulk $YBa_2Cu_3O_x$ superconductor. Appl. Phys. Lett. **54**, 2352–2354 (1989)
21. Y. Zalaoglu, U. Erdem, F.C. Bolat, B. Akkurt, T. Turgay, G. Yildirim, Improvement in fundamental electronic properties of Bi-2212 electroceramics with trivalent Bi/Tm substitution: a combined experimental and empirical model approach. J. Mater. Sci. **20**, 1–13 (2021)
22. M.B. Turkoz, M. Oz, T. Turgay, G. Yildirim, Gece Kitapligi, Evaluation of magneto-resistivity performances and flux pinning centers with vanadium addition in Bi-2223 main matrix, pp. 139 -158, Ankara
23. A.M. Luiz, *Applications of High-Tc Superconductivity* (Janeza Trdine, Rijeka, 2011)
24. J.D. Hodge, H. Muller, D.S. Applegate, Q. Huang, A resistive fault current limiter based on high temperature superconductors. Appl. Supercond. **3**, 469–482 (1995)
25. Y. Zalaoglu, G. Yildirim, C. Terzioglu, Magnetoresistivity study on Cr added Bi-2212 superconductor ceramics with experimental and theoretical approaches. J. Mater. Sci. **24**, 239–247 (2013)
26. S.E.M. Ghahfarokhi, M.Z. Shoushtari, Structural and physical properties of Cd-doped Bi1. 64Pb0. 36Sr2Ca2− xCdxCu3Oy superconductor. Physica B **405**, 4643–4649 (2010)
27. J. Tarascon, W. McKinnon, P. Barboux, D. Hwang, B. Bagley, L. Greene et al., Preparation, structure, and properties of the superconducting cuprate series $Bi_2Sr_2Ca_{n-1}Cu_nO_y$ with n=1, 2, and 3. Phys. Rev. B **38**(13), 8885–8892 (1988)
28. J. Emsley, *Nature's Building Blocks: An A-Z Guide to the Elements* (Oxford University Press, Oxford, 2001), pp. 181–182
29. C.K. Gupta, N. Krishnamurthy, *Extractive Metallurgy of Rare Earths* (CRC Press, Boca Raton, 2004)
30. D. Jiles, *Introduction to Magnetism and Magnetic Materials* (CRC Press, Boca Raton, 1998)
31. O. Ozturk, E. Asikuzun, G. Yildirim, The role of Lu doping on microstructural and superconducting properties of Bi 2 Sr 2 CaLu x Cu 2 O y superconducting system. J. Mater. Sci. **24**(4), 1274–1281 (2013)
32. W. Abdeen, S. Marahba, R. Awad, A.I. Abou Aly, I.H. Ibrahim, M. Matar, Electrical and mechanical properties of (Bi, Pb)-2223 substituted by holmium. J. Adv. Ceram. **5**(1), 54–69 (2016)
33. Z. Chen, L. Yang, X. Wang, H. Yin, High magneto-optical characteristics of Holmium-doped terbium gallium garnet crystal. Opt. Lett. **41**(11), 2580–2583 (2006)

34. Y. Sakabe, Y. Hamaji, H. Sano, N. Wada, Effects of rare-earth oxides on the reliability of X7R dielectrics. Jpn. J. Appl. Phys. **41**, 5668–5679 (2002)
35. H. Saito, H. Chazono, H. Kishi, N. Yamaoka, X7R Multilayer ceramic capacitors with nickel electrodes. Jpn. J. Appl. Phys. **30**, 2307–2310 (2001)
36. E. Celik, High temperature Ho 2 O 3–ZrO 2 insulation coatings on AgMg sheathed Bi-2212 superconducting tapes by sol–gel technique for magnet technology. J. Sol-Gel. Sci. Technol. **53**(3), 561–569 (2010)
37. N.K. Saritekin, Y. Zalaoglu, G. Yildirim, M. Dogruer, C. Terzioglu, A. Varilci, O. Gorur, Determination of solid solubility level of Ho nanoparticles in Y-123 superconducting matrix and strong Cu-1 site preference of nanoparticles. J. Alloys Comp. **610**, 361–371 (2014)
38. S. Vinu, P.M. Sarun, A. Biju, R. Shabna, P. Guruswamy, U. Syamaprasad, The influence of sintering temperature on the microstructure and superconducting properties of $Bi_{1.7}Pb_{0.4}Sr_{1.8}Nd_{0.2}Ca_{1.1}Cu_{2.1}O_{8+delta}$ superconductor. Supercond. Sci. Technol. **21**, 045001–045005 (2008)
39. R. Shabna, P.M. Sarun, S. Vinu, A. Biju, U. Syamaprasad, Doping controlled metal to insulator transition in the (Bi, Pb)-2212 system. Supercond. Sci. Technol. **22**, 045016–045022 (2009)
40. V. Mihalache, I.G. Deac, A.V. Pop, L. Miu, The pinning force density in polycrystalline $Bi_{1.8}Pb_{0.4}Sr_2Ca_{2-x}Y_xCu_3O_y$ multiphase systems. Curr. Appl. Phys. **11**, 1010–1014 (2011)
41. D. Marconi, G. Stiufiuc, A.V. Pop, Effect of partial substitution of Ca by 4f elements on dissipative processes in Bi:2223 superconductors. J. Phys. Conf. Ser. **153**, 012022 (2009)
42. S. Vinu, P.M. Sarun, A. Biju, R. Shabna, P. Guruswamy, U. Syamaprasad, The effect of substitution of Eu on the critical current density and flux pinning properties of (Bi, Pb)-2212 superconductor. Supercond. Sci. Technol. **21**, 045001–045005 (2008)
43. S. Razia, S.P. Murikoli, V. Surendran, S. Upendran, Doping dependent metal to insulator transition in the (Bi, Pb)-2212 system: The evolution of structural and electronic properties with europium substitution. Chin. Phys. B **18**(9), 4000 (2009)
44. P.M. Sarun, S. Vinu, R. Shabna, A. Biju, U. Syamaprasad, Microstructural and superconducting properties of Yb-substituted (Bi, Pb)-2212 superconductor sintered at different temperatures. J. Alloys Compd. **472**, 13–17 (2009)
45. A. Biju, P.M. Sarun, R.P. Aloysius, U. Syamaprasad, Flux pinning properties of Yb substituted (Bi, Pb)-2212 superconductor. J. Alloys Compd. **454**, 46–51 (2008)
46. R.J. Sanderson, K.C. Hewitt, Stoichiometry control of magnetron sputtered $Bi_2Sr_2Ca_{1-x}Y_xCu_2O_y$ $(0 \leqslant x \leqslant 0.5)$ thin film, composition spread libraries: Substrate bias and gas density factors. Physica C **425**, 52–61 (2005)
47. G. Yildirim, Formation of artificial flux pinning centers in Bi-2223 cuprate superconductor with Ni impurities and enhanced resistant to thermal fluxon motions of correlated 2D pancake vortices in new matrix. J. Alloys Compd. **745**, 100–110 (2018)
48. C. Nguyen-Van-Huong, C. Hinnen, J.M. Siffre, Superconductivity and X-ray photoelectron spectroscopy studies of $Bi_2Sr_{2-x}La_xCaCu_2O_{8+\delta}$. J. Mater. Sci. **32**, 1725–1731 (1997)
49. Y. Zalaoglu, G. Yildirim, C. Terzioglu, O. Gorur, Detailed analysis on electrical conduction transition from 2D variable range hopping to phonon-assisted 3D VRH mechanism belonging to Bi-site La substituted Bi-2212 system. J. Alloys Compd. **622**, 489–499 (2015)
50. B.D. Cullity, S.R. Stock, *Elements of X-Ray Diffraction*, 3rd edn. (Pearson, Harlow, 2014)
51. W. Gao, J.B. Vander-sande, Textured BSSCO/Ag superconducting microcomposites with improved critical current-density through mechanical deformation. Supercond. Sci. Technol. **5**, 318–326 (1992)
52. F.K. Lotgering, Topotactical reactions with ferrimagnetic oxides having hexagonal crystal structures–I. J. Inorg. Nucl. Chem. **9**, 113–123 (1959)
53. N.K. Saritekin, M. Pakdil, E. Bekiroglu, G. Yildirim, Examination of effective nucleation centers for flux pinning of vortices and optimum diffusion annealing temperature for Au-diffusion-doped Bi-2212 polycrystalline compound. J. Alloys Compd. **688**, 637–646 (2016)
54. A. Sotelo, M.A. Madre, J.C. Diez, S. Rasekh, L.A. Angurel, E. Martinez, The influence of Pb and Ag doping on the Jc (H, T) dependence and the mechanical properties of Bi-2212 textured rods. Supercond Sci Technol **22**(3), 034012 (2009)
55. K. Kocabas, M. Ciftcioglu, The effect of Sb substitution of Cu in $Bi_{1.7}Pb_{0.3}Sr_2Ca_2Cu_{3-x}Sb_xO_y$ superconductors. Phys. Status Solidi A **177**, 539–545 (2000)
56. C.J. Poole, H.A. Farach, R. Creswick, *Superconductivity* (Academic Press, San Diego, 1995)
57. R.R. Reddy, M. Murakami, S. Tanaka, P.V. Reddy, Elastic behavior of a Y-Ba-Cu-O sample prepared by the MPMG method. Physica C **257**, 137–142 (1996)
58. M. Li, Y. Zhang, Y. Li, Y. Qi, Granular superconductivity in polycrystalline $Bi_2Sr_2CaCu_2O_{8+\gamma}$ by homovalent La substitution on Bi sites. J. Non-Cryst. Solids **356**, 2831–2835 (2010)
59. X. Xu, J.H. Kim, S.X. Dou, S. Choi, J.H. Lee, H.W. Park, M. Rindfleish, M. Tomsic, A correlation between transport current density and grain connectivity in MgB2/Fe wire made from ball-milled boron. J. Appl. Phys. **105**, 103913 (2009)

60. M.B. Turkoz, Y. Zalaoglu, T. Turgay, O. Ozturk, B. Akkurt, G. Yildirim, Evaluation of key mechanical design properties and mechanical characteristic features of advanced Bi-2212 ceramic materials with homovalent Bi/Ga partial replacement: Combination of experimental and theoretical approaches. Ceram. Int. **45**(17), 21183–21192 (2019)
61. P.B. Allen, Y.E. Picket, H. Krakauer, Phys. Rev. B **37**, 7482–7490 (1988)
62. M.B. Turkoz, M. Oz, T. Turgay, G. Yıldırım, Evaluatıon of Magneto-Resistivity Performances and Flux Pinning Centers With Vanadium Addition in Bi-2223 main matrix. Theory Res Sci Math **2**, 139 (2017)
63. M.B. Turkoz, S. Nezir, C. Terzioglu, A. Varilci, G. Yildirim, Investigation of Lu effect on $YBa_2Cu_3O_{7-\gamma}$ superconducting compounds. J. Mater. Sci **24**, 896–905 (2013)
64. S. Martin, M. Gurvitch, C.E. Rice, A.F. Hebard, P.L. Gammel, R.M. Fleming, A.T. Fiory, Nonlinear temperature-dependence of the normal-state resistivity in $YBa_2Cu_4O_{8\gamma}$ films. Phys. Rev. B **39**, 9611–9613 (1989)
65. R. Shabna, P.M. Sarun, S. Vinu, U. Syamaprasad, Charge carrier localization and metal to insulator transition in cerium substituted (Bi, Pb)-2212 superconductor. J. Alloys Compd. **493**, 11–16 (2010)
66. D.M. Newns, P.C. Pattnaik, C.C. Tsuei, Role of vanhove singularity in high-temperature superconductors: mean field. Phys. Rev. B **43**, 3075–3084 (1991)
67. M.B. Turkoz, Y. Zalaoglu, T. Turgay, O. Ozturk, G. Yildirim, Effect of homovalent Bi/Ga substitution on propagations of flaws, dislocations and crack in Bi-2212 superconducting ceramics: Evaluation of new operable slip systems with substitution. Ceram. Int. **45**(17), 22912–22919 (2019)
68. J. Ekin, *Experimental Techniques for Low-Temperature Measurements: Cryostat Design, Material Properties and Superconductor Critical-Current Testing* (Oxford University Press, New York, 2006)
69. P. Kovac, I. Hušek, W. Pachla, T. Melišek, R. Diduszko, K. Fröhlich, A. Morawski, A. Presz, D. Machajdik, Structure, grain connectivity and pinning of as-deformed commercial MgB2 powder in Cu and Fe/Cu sheaths. Supercond. Sci. Technol. **15**(7), 1127 (2002)
70. T. Turgay, G. Yildirim, Effect of aliovalent Si/Bi partial substitution on propagation mechanisms of cracking and dislocation in Bi-2212 crystal system. J. Mater. Sci. **30**(8), 7314–7323 (2019)
71. M. Dogruer, C. Aksoy, G. Yildirim, O. Ozturk, C. Terzioglu, Influence of Sr/Nd partial replacement on fundamental properties of Bi-2223 superconducting system. J. Mater. Sci **32**, 7073–7089 (2021)
72. R. Awad, A.I. Abou-Aly, M.M.H.A. Gawad, I. G-Eldeen, The influence of $SnO_2$ nano-particles addition on the vickers microhardness of (Bi, Pb)-2223 superconducting phase. J. Supercond. Nov. Magn. **25**, 739–745 (2012)
73. M. Sahoo, D. Behera, Effect of Ti doping on structural and superconducting property of YBa2Cu3O7−y high Tc Superconductor. J. Supercond. Nov. Magn. **27**, 83–93 (2014)
74. N.K. Sartekin, M. Pakdil, G. Yildirim, M. Oz, T. Turgay, Decrement in metastability with Zr nanoparticles inserted in Bi-2223 superconducting system and working principle of hybridization mechanism. J. Mater. Sci **27**, 956–965 (2016)
75. M. Dogruer, G. Yildirim, E. Yucel, C. Terzioglu, Role of diffusion-annealing temperature on the microstructural and superconducting properties of Cu-doped $MgB_2$ superconductors. J. Mater. Sci. **23**, 1965–1970 (2012)